ISSN 1560-3547, Regular and Chaotic Dynamics, 2013, Vol. 18, No. 5, pp. 508–520. © Pleiades Publishing, Ltd., 2013.

Strange Attractors and Mixed Dynamics in the Problem of an Unbalanced Rubber Ball Rolling on a Plane

Alexey O. Kazakov*

Institute of computer science
ul. Universitetskaya 1, Izhevsk, 426034, Russia
The Research Institute of Applied Mathematics and Cybernetics,
Nizhny Novgorod State University,
pr. Gagarina 23, Nizhny Novgorod, 603950, Russia
Received May 30, 2013; accepted September 3, 2013

Abstract—We consider the dynamics of an unbalanced rubber ball rolling on a rough plane. The term *rubber* means that the vertical spinning of the ball is impossible. The roughness of the plane means that the ball moves without slipping. The motions of the ball are described by a nonholonomic system reversible with respect to several involutions whose number depends on the type of displacement of the center of mass. This system admits a set of first integrals, which helps to reduce its dimension. Thus, the use of an appropriate two-dimensional Poincaré map is enough to describe the dynamics of our system. We demonstrate for this system the existence of complex chaotic dynamics such as strange attractors and mixed dynamics. The type of chaotic behavior depends on the type of reversibility. In this paper we describe the development of a strange attractor and then its basic properties. After that we show the existence of another interesting type of chaos — the so-called mixed dynamics. In numerical experiments, a set of criteria by which the mixed dynamics may be distinguished from other types of dynamical chaos in two-dimensional maps is given.

MSC2010 numbers: 37J60, 37N15, 37G35

DOI: 10.1134/S1560354713050043

Keywords: mixed dynamics, strange attractor, unbalanced ball, rubber rolling, reversibility, two-dimensional Poincaré map, bifurcation, focus, saddle, invariant manifolds, homoclinic tangency, Lyapunov's exponents.

On the occasion of the 60th birthday of my advisor S. V. Gonchenko, a prominent scientist and an outstanding man!

1. INTRODUCTION

This paper complements a series of works devoted to the study of a new, poorly known type of motion — *rubber rolling* and describes the motions of a dynamically asymmetric ball with a displaced center of mass on a plane. The term *rubber* was first proposed with respect to motions in [1, 2], but this type of motions had been considered more than a century ago by J. Hadamard [3]. For more information see the recently published paper [4], which presents the results of investigations of the integrability of a system governing the motion of a rubber body (a ball or an ellipsoid) on a plane or a sphere. These problems are also dealt with in [5], where special cases of integrability of the problem of the motion of a rubber ellipsoid on a plane and a sphere are considered by combining analytical and numerical approaches.

There are two reasons for the increased interest in rubber body dynamics. On the one hand, such motions are to investigate numerically than the motions with spinning. Systems with rubber rolling admit an additional integral, which helps to reduce the analysis of such problems to the

*E-mail: kazakovdz@yandex.ru

investigation of the two-dimensional Poincaré map. On the other hand, such an idealization can be achieved in real experiments. To do this, the body should have a rubber surface.

However, even the dynamics in such systems turns out to be very rich and complex. An integrable case was pointed out only in [6], when two principal moments of inertia are equal and the center of mass of the ball is displaced only along one principal axis of inertia. Moreover, in [7] it is proved that a system governing the motion of an unbalanced rubber ball (with one non-zero component of displacement) on a plane has no an *invariant measure* even in the case of a full set of first integrals (when the acceleration of gravity is zero). If the acceleration of gravity is non-zero, the *additional integral* disappears and the absence of an *invariant measure* becomes obvious from the analysis of the Poincaré map.

The main goal of the paper is to demonstrate the richness and complexity of the dynamics of an unbalanced rubber ball on a plane rather than investigating all dynamical properties in detail.

2. EQUATIONS OF A MOTION AND FIRST INTEGRALS

Consider the motion of an unbalanced rubber ball on a plane. There is no *slipping* and *spinning* at the contact point of the ball with the plane. These conditions are governed by *nonholonomic constraints* represented as:

$$\boldsymbol{v} + \boldsymbol{\omega} \times \boldsymbol{r} = 0, \quad (\boldsymbol{\omega}, \boldsymbol{\gamma}) = 0, \tag{2.1}$$

where $\boldsymbol{r}$ is the radius vector connecting the center of mass with the contact point P, $\boldsymbol{v}$ and $\boldsymbol{\omega}$ are the velocity of the center of mass and the angular velocity of the ball, respectively, and $\boldsymbol{\gamma}$ is the normal unit vector of the plane at the contact point (see Fig. 1). Note that $\boldsymbol{r}$, $\boldsymbol{v}$, $\boldsymbol{\omega}$ and $\boldsymbol{n}$ are projected onto the moving axes Cx, Cy and Cz attached to the ball.

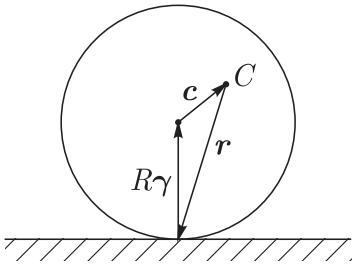

Fig. 1. An unbalanced ball on a plane.

The equations governing the evolution of $\boldsymbol{\omega}$ and $\boldsymbol{\gamma}$ in the gravity field can be represented as:

$$\begin{cases} \tilde{\mathbf{I}}\dot{\boldsymbol{\omega}} = (\tilde{\mathbf{I}}\boldsymbol{\omega}) \times \boldsymbol{\omega} - m\boldsymbol{r} \times (\boldsymbol{\omega} \times \dot{\boldsymbol{r}}) + ma_g(\boldsymbol{\gamma} \times \boldsymbol{a}) + \lambda_0(a_g)\boldsymbol{\gamma} \\ \dot{\boldsymbol{\gamma}} = \boldsymbol{\gamma} \times \boldsymbol{\omega}, \end{cases} \tag{2.2}$$

where $\tilde{\mathbf{I}} = \mathbf{I} + m(\boldsymbol{r}, \boldsymbol{r}) \cdot \mathbf{E} - m\boldsymbol{r} \cdot \boldsymbol{r}^{\boldsymbol{T}}$ is the tensor of inertia relative to the point of contact, m is the mass of the ball and a_g is the acceleration of gravity, $\mathbf{I} = diag(I_1, I_2, I_3)$, where I_1, I_2, I_3 are the principal moments of inertia relative to the moving axes Cx, Cy and Cz.

For the unbalanced ball the vectors $\boldsymbol{r}$ and $\boldsymbol{\gamma}$ are related by $\boldsymbol{r} = -R\boldsymbol{\gamma} - \boldsymbol{a}$, where $\boldsymbol{a}$ is the displacement of the center of mass with the components (a_1, a_2, a_3).

The undetermined multiplier λ_0 is responsible for the rubber constraints $(\boldsymbol{\omega}, \boldsymbol{\gamma}) = 0$ and can be represented as

$$\lambda_0(a_g) = -\frac{\left(\tilde{\mathbf{I}}^{-1}\boldsymbol{\gamma}, (\tilde{\mathbf{I}}\boldsymbol{\omega}) \times \boldsymbol{\omega} - m\boldsymbol{r} \times (\boldsymbol{\omega} \times \dot{\boldsymbol{r}}) + ma_g(\boldsymbol{\gamma} \times \boldsymbol{a})\right)}{(\boldsymbol{\gamma}, \tilde{\mathbf{I}}^{-1}\boldsymbol{\gamma})}. \tag{2.3}$$

Equations (2.2) admit three *first integrals*:

$$\mathcal{E} = \frac{1}{2}(\boldsymbol{\omega}, \tilde{\mathbf{I}}\boldsymbol{\omega}) - ma_g(\boldsymbol{r}, \boldsymbol{\gamma}), \quad (\boldsymbol{\gamma}, \boldsymbol{\gamma}) = 1, \quad (\boldsymbol{\omega}, \boldsymbol{\gamma}) = 0. \tag{2.4}$$

The energy and geometric integrals are common for all nonholonomic problems. The third integral is specified by rubber constraints (in what follows we will call it *rubber integral*). Thus, by the *Euler–Jacobi theorem* for integrability of the system (2.2) the existence of an *invariant measure* and an additional *fourth integral* is necessary. Such additional invariants exist in the case $I_1 = I_2, a_1 = a_2 = 0$. Moreover, in [6] it is proved that this system can be represented in a conformally Hamiltonian form.

An additional integral also exists in the case of arbitrary parameters $\boldsymbol{I}, \boldsymbol{a}$, when $a_g = 0$. But in this case the system (2.2) is not integrable due to the absence of an invariant measure (see [7]).

For arbitrary values of the parameters the system (2.2) admits neither an additional integral nor an invariant measure. Due to these facts the dynamics of the system turns out to be very rich and complex.

3. THE POINCARÉ MAP

As in most problems of nonholonomic mechanics, it is very convenient to use the Poincaré cross-sections for numerical investigation of the system under consideration. On the common level set of three integrals (2.4) our system can be restricted to the three-dimensional manifold

$$\mathcal{M}^3 = \{(\boldsymbol{\omega}, \boldsymbol{\gamma}) : (\boldsymbol{\gamma}, \boldsymbol{\gamma}) = 1, (\boldsymbol{\omega}, \boldsymbol{\gamma}) = 0, E(\boldsymbol{\omega}, \boldsymbol{\gamma}) = const\}. \tag{3.1}$$

For parametrization of this manifold we use special variables (L, G, l, g), which can be represented as:

$$\begin{gathered}
\omega_1 = \sqrt{G^2 - L^2}\sin l, \\
\omega_2 = \sqrt{G^2 - L^2}\cos l, \\
\omega_3 = L, \\
\gamma_1 = \frac{L}{G}\ \cos g \sin l + \sin g \cos l, \\
\gamma_2 = \frac{L}{G}\ \cos g \cos l - \sin g \sin l, \\
\gamma_3 = -\sqrt{1 - \left(\frac{L}{G}\right)^2}\ \cos g.
\end{gathered} \tag{3.2}$$

Remark 1. Similar variables are used for many problems of nonholonomic and rigid body dynamics (see, for example, [8]), where they are called the Andoyer–Deprit variables.

Note that in the new variables the geometric and rubber integrals are conserved automatically. Hence, Eqs. (3.2) specify one-to-one transformations everywhere except for $L/G = \pm 1$. As a secant for this flow we choose a manifold given by

$$g = g_0 = \text{const}.$$

The cross-section of the three-dimensional manifold $\mathcal{M}^3$ formed by the intersection with the secant $g = g_0$ forms the two-dimensional Poincaré map

$$\begin{gathered}
\mathcal{F}_{g_0} : \mathcal{M}^2_{g_0} \to \mathcal{M}^2_{g_0}, \\
\mathcal{M}^2_{g_0} = \{x \in \mathcal{M}^3 | g(x) = g_0\},
\end{gathered} \tag{3.3}$$

which is defined on $\mathbb{S}^2$. For parametrization of $\mathcal{M}^2_{g_0}$ we use the variables $l \mod 2\pi$ and $\frac{L}{G} \in [-1, 1]$. Thus, the pair $(l, \frac{L}{G})$ defines a point in $\mathbb{S}^2$ on which the Poincaré map $\mathcal{F}_{g_0}$ is applied.

Remark 2. In the problems of "classical" rolling with spinning the Poincaré cross-section is three-dimensional [9, 10] and hence more difficult to analyze.

4. REVERSIBILITY OF THE FLOW AND THE MAP

Our investigation shows that the dynamics of the system under consideration significantly depends on the type of *reversibility*. We represent the equations of motion (2.2) as $\dot{\boldsymbol{X}} = \boldsymbol{v}(\boldsymbol{X})$, where $\boldsymbol{X} = (\omega_1, \omega_2, \omega_3, \gamma_1, \gamma_2, \gamma_3)$. Recall that the map of the phase space $R(\boldsymbol{X}) : \boldsymbol{X} \to \boldsymbol{X}$ is called *involution for the flow* $\boldsymbol{v}(\boldsymbol{X})$ if

$$\frac{dR(\boldsymbol{X})}{dt} = -\boldsymbol{v}(R(\boldsymbol{X})), R \circ R = id. \tag{4.1}$$

In this case the flow $\boldsymbol{v}(\boldsymbol{X})$ is called *reversible* with respect to the *involution* $R(\boldsymbol{X})$.

In the system (2.2) there exists the *trivial involution*

$$R_0 : \boldsymbol{\omega} \to -\boldsymbol{\omega}, \boldsymbol{\gamma} \to \boldsymbol{\gamma}, t \to -t, \tag{4.2}$$

which reverses the angular velocities of the system. The set of fixed points of this involution is the subspace of zero angular velocities ($\omega_1 = \omega_2 = \omega_3 = 0$). In addition to the *trivial involution*, the system admits additional involutions, whose number is defined by the number of non-zero components of the displacement of the center of mass.When the ball is balanced ($a_1 = a_2 = a_3 = 0$), the system has the maximal number of involutions. Depending on the type of transformation of the evolution variables $(\boldsymbol{\omega}, \boldsymbol{\gamma})$, all additional involutions can be divided into two classes:

- involutions corresponding to the rotation of the ball by the angle π about one of three axes attached to this ball

$$\begin{aligned} &\Pi_1 : \boldsymbol{\omega} \to (\omega_1, \omega_2, -\omega_3), && \boldsymbol{\gamma} \to (-\gamma_1, -\gamma_2, \gamma_3), && t \to -t \\ &\Pi_2 : \boldsymbol{\omega} \to (\omega_1, -\omega_2, \omega_3), && \boldsymbol{\gamma} \to (-\gamma_1, \gamma_2, -\gamma_3), && t \to -t \\ &\Pi_3 : \boldsymbol{\omega} \to (-\omega_1, \omega_2, \omega_3), && \boldsymbol{\gamma} \to (\gamma_1, -\gamma_2, -\gamma_3), && t \to -t \end{aligned} \tag{4.3}$$

- involutions corresponding to the reflection of the ball with respect to one of three planes passing through a pair of the axes attached to the ball

$$\begin{aligned} &\Sigma_1 : \boldsymbol{\omega} \to (\omega_1, \omega_2, -\omega_3), && \boldsymbol{\gamma} \to (\gamma_1, \gamma_2, -\gamma_3), && t \to -t \\ &\Sigma_2 : \boldsymbol{\omega} \to (\omega_1, -\omega_2, \omega_3), && \boldsymbol{\gamma} \to (\gamma_1, -\gamma_2, \gamma_3), && t \to -t \\ &\Sigma_3 : \boldsymbol{\omega} \to (-\omega_1, \omega_2, \omega_3), && \boldsymbol{\gamma} \to (-\gamma_1, \gamma_2, \gamma_3), && t \to -t \end{aligned} \tag{4.4}$$

If the center of mass of the ball is displaced only along one axis, then the system (2.2) admits three involutions (in addition to R_0): the involution corresponding to the rotation of the ball by the angle π along the axis of displacement (one of Π_i, $i = 1, \ldots, 3$) and two involutions corresponding to the reflection of the ball with respect to the planes passing through the axis of displacement and another axis (two from Σ_i, $i = 1, \ldots, 3$). If the center of mass of the ball is displaced along two axes, then the system (2.2) admits only one additional involution corresponding to the reflection of the ball with respect to the plane passing through these axes. In the case of arbitrary displacement of the center of mass (when all components a_1, a_2 and a_3 are non-zero) the system under consideration does not admit additional involutions.

We now recall the definitions of reversibility and involution for maps. The transformation $r(\boldsymbol{x}) : \boldsymbol{x} \to \boldsymbol{x}$ is called *involution for the map* (3.3) if

$$\mathcal{F}_{g_0} \circ r = r \circ \mathcal{F}_{g_0}^{-1}. \tag{4.5}$$

The map $\mathcal{F}_{g_0}(\boldsymbol{x})$ is called *reversible* with respect to the *involution* $r(\boldsymbol{x})$.

It is clear that every involution for a flow system can be reduced to the involution of its Poincaré map if a manifold invariant under this involution is chosen as a secant.

In what follows, such involutions reduced from the flow system to the Poincaré cross-section (3.3) will be called *reduced involutions*. For the Poincaré map (3.3) the *reduced involutions* can be represented as

- Reduced R_0:

$$r_0 : \frac{L}{G} \to -\frac{L}{G}, \qquad l \to l + \pi, \qquad g \to -g \tag{4.6}$$

- Reduced Π_1, Π_2 and Π_3

$$\begin{aligned} &\pi_1 : \frac{L}{G} \to -\frac{L}{G}, && l \to l, && g \to -g \\ &\pi_2 : \frac{L}{G} \to \frac{L}{G}, && l \to \pi - l, && g \to \pi - g \\ &\pi_3 : \frac{L}{G} \to \frac{L}{G}, && l \to -l, && g \to \pi - g \end{aligned} \tag{4.7}$$

- Reduced Σ_1, Σ_2 and Σ_3

$$\begin{aligned} &\sigma_1 : \frac{L}{G} \to -\frac{L}{G}, && l \to l, && g \to \pi - g \\ &\sigma_2 : \frac{L}{G} \to \frac{L}{G}, && l \to \pi - l, && g \to -g \\ &\sigma_3 : \frac{L}{G} \to \frac{L}{G}, && l \to -l, && g \to -g \end{aligned} \tag{4.8}$$

For each involution (except for r_0) the set of fixed points is represented as lines in the variables (L, G, l, g). Hereafter we will call such lines the *lines of fixed points* or *fixed lines*. For the involution r_0 the set of fixed points is undefined because of uncertainty of the variables (L, G, l, g), when the angular velocities are zero. Due to the involution r_0 the phase portraits in the Poincaré map preserve an obvious symmetry, according to which each trajectory in the map has a symmetrical analog. Thus, for each stable trajectory the system under consideration has a symmetrical unstable trajectory.

It is well known from [11, 12] that the behavior of reversible systems in a neighborhood of the intersection of the images of the Poincaré map for *fixed lines* (hereafter *images of fixed lines*) is close to a conservative, i.e, area-preserving behavior. This property helps to search for regions with possible dissipation by analyzing the behavior of *images of fixed lines*.

The intersections of various *images of fixed lines* contain conservative periodic points (elliptic or saddle points with unit saddle values). Hence, the system near such points is mostly area-preserving [13]. The regions without such points can contain *sinks* and *sources* such as fixed or periodic points, invariant curves and even strange attractors.

When the Poincaré map is reversible with respect to several involutions with *fixed lines*, the network of the *images of fixed lines* can be very dense. Thus, the dynamical behavior in the system (2.2) becomes more complex from the case of the maximal number of involutions (balanced ball) to the case with only *trivial involution* r_0 (completely unbalanced ball, when the displacement of the center of mass has three non-zero components).

In this paper we consider two cases in detail.

- The case of a completely unbalanced ball: the system (Poincaré map) reversible with respect to only one involution R_0 (r_0).
- The case of a partially unbalanced ball (two of three components of the displacement are non-zero and the third component is zero): the system (Poincaré map) is reversible with respect to two involutions R_0 (r_0) and one of Σ_i (σ_i), $i = 1 \dots 3$.

5. STRANGE ATTRACTORS

The problem of an unbalanced rubber ball rolling on a plane is not the first nonholonomic problem where strange attractors were found. Not long ago strange attractors were found in the *nonholonomic model of a Celtic stone* [14, 15]. The papers [16, 17] are also devoted to investigations of strange attractors in this model. In [17] the *spiral strange attractor of Shilnikov* was discovered in the *nonholonomic model of a Celtic stone*. The scenario of development of this strange attractor was also presented in [18]. Some more strange attractors were found in the above-mentioned model in [16], where they were investigated using numerical calculations. Quite recently the "famous" *strange attractor of Lorenz type* has been discovered in the same model of the Celtic stone [18]. Remarkably, this model is the first model from applications where the Lorenz-like attractor was found.

5.1. Development of a Strange Attractor

In the case of a completely unbalanced ball, strange attractors can exist in the system (2.2). Fig. 2 shows one of such attractors for the following values of parameters:

$$\begin{gathered} E = 50, R = 3, m = 1, \\ I_1 = 1, I_2 = 2, I_3 = 3, \\ a_1 = 1, a_2 = 1.5, a_3 = 0.5, \\ g = 0. \end{gathered} \tag{5.1}$$

Remark 3. Note that the triangle inequality for the principal moments of inertia I_1, I_2 and I_3 does not hold strictly. But this does not matter in our case, since the main goal of this paper is to demonstrate the richness and complexity of the dynamics of the system (2.2). Moreover, strange attractors were also found for a wide range of parameters of the system (when the triangle inequality holds strictly), but for the values (5.1) the attractor looks particularly clear.

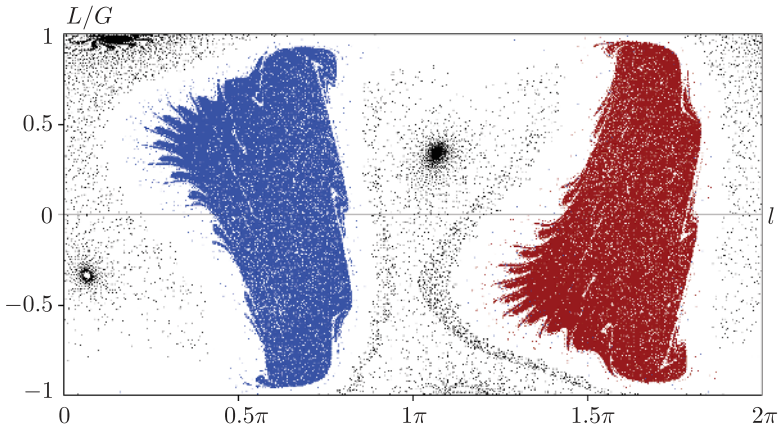

Fig. 2. The Poincaré map of a *strange attractor* and a *strange repeller*. The chaotic set on the left is a strange attractor and its symmetric (with respect to the involution r_0) analog is a strange repeller on the right. Almost all trajectories starting from the repeller evolve onto the attractor with a small number of iterations.

Let us describe the development of the strange attractor from Fig. 2. We consider the acceleration of gravity a_g as a bifurcational parameter. Note that the energy parameter E can be used as a bifuractional parameter instead of a_g, since the increase in the value of a_g is equal to the decrease in the total energy of the system.

The development of the strange attractor is a rather complicated process and is associated with a series of *local* and *global bifurcations*. By the *local bifurcations* we mean (as usual) bifurcations of fixed and periodic points and bifurcations of invariant curves on the Poincaré map. Among the *global bifurcations* we will take into account those resulting in qualitative changes of the regions of attraction (repulsion) of invariant sets (fixed or periodic points or invariant curves), which are related to evolutions of the invariant manifolds of saddle points.

The main stages of development of the *strange attractor* are described below (for more details see [19]).

- When $a_g = 0$, the phase portrait in the Poincaré map looks area-preserving. The invariant curves surround the elliptic points F_l, F_r, F_d and F_t separated by two saddle points S_l and S_r (see Fig. 3a). When the parameter a_g becomes positive, the elliptic points become foci and most of invariant curves are destroyed. When $a_g > 7.58$, the region of attraction of the focus F_l (hereafter referred as the region $\mathfrak{L}$) are bounded by the unstable invariant manifold of the saddle S_r. Due to the involution r_0 the region $\mathfrak{R} = r_0(\mathfrak{L})$ is bounded by the stable invariant manifold of the saddle S_l (see Fig. 3b).

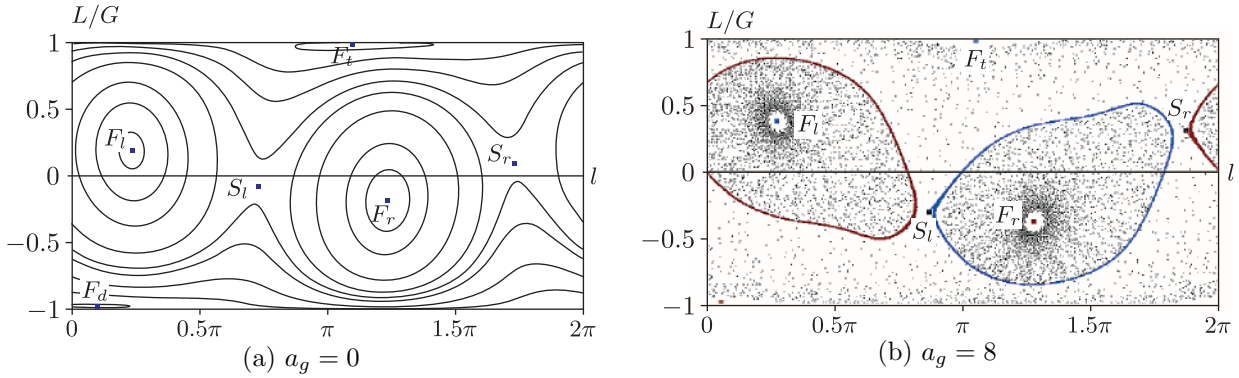

Fig. 3. Poincaré maps. a) The phase portrait is foliated into invariant curves which surround the elliptic points F_l, F_r, F_d and F_t separated by two saddle points S_l and S_r. b) Elliptic points become foci. F_l and F_t are stable foci, while F_r and F_t are unstable foci. A stable invariant manifold of the saddle S_r is coiled around the focus F_l, while an unstable invariant manifold of S_l is coiled around F_r.

- When $a_g \simeq 8.65$, saddle-node bifurcations occur. The stable node point F_n and the saddle point S_n are born in $\mathfrak{L}$, and (due to the involution r_0) an unstable node and a saddle are born in $\mathfrak{R}$ (see Fig. 4a). The node F_n very soon becomes a focus. When $a_g > 8.85$, stable and unstable manifolds of the saddle S_n form a *homoclinic figure-eight* [20]. Thus, both stable manifolds of S_n are intersected by its unstable manifold, while the second unstable manifold is coiled around the focus F_l (see Fig. 4c). Such intersections lead to the onset of chaos in a neighborhoods of S_n.

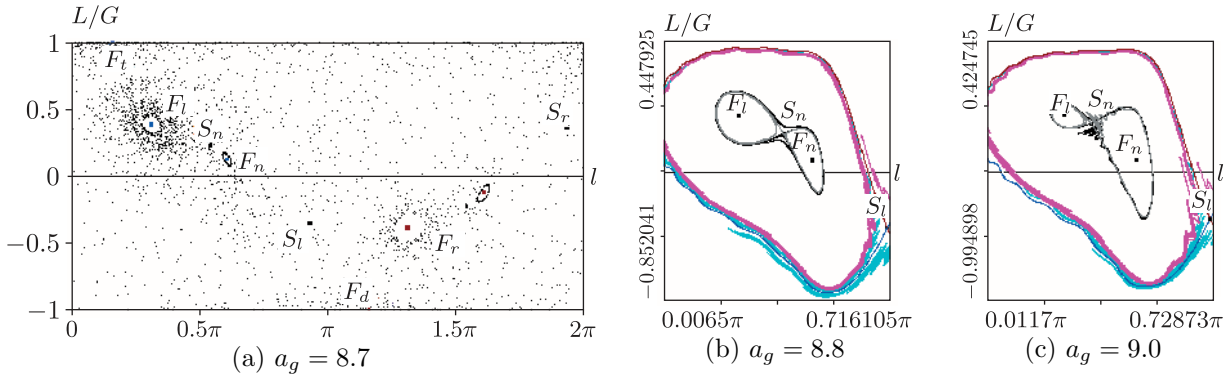

Fig. 4. Poincaré maps. a) Saddle-node bifurcation for $a_g \simeq 8.65$. The stable focus F_n and the saddle S_n are born in the region $\mathfrak{L}$. b-c) Behavior of stable (black) and unstable (gray) invariant manifolds of the saddle S_n. The region containing F_l, S_n and F_n is bounded by the unstable invariant manifold of S_r.

- As a_g increases, the saddle S_n approaches the focus F_l and, when $a_g \simeq 9.14$, disappears due to a saddle-node bifurcation. But the chaos in the region $\mathfrak{L}$ exists as before, because the *saddle node with a transversal homoclinic vanishes* [21]. Thereafter, the focus F_n is only one fixed point in the region $\mathfrak{L}$. Starting with $a_g \simeq 8.94$ F_n loses stability due to a *cascade of local bifurcations*, after which only saddle points remain in the region $\mathfrak{L}$. This cascade seems interesting and will be described in Section 5.1.1.

- When $a_g \simeq 9.77$, the final evolution of the invariant manifolds of S_l and S_r occurs (see Fig. 5), after which almost all trajectories evolve from the region $\mathfrak{R}$ into the region $\mathfrak{L}$ with positive iterations of the Poincaré map. Thus, the attractive set in $\mathfrak{L}$ is a *strange attractor* and the symmetric repulsion set in $\mathfrak{R}$ is a *strange repeller*.

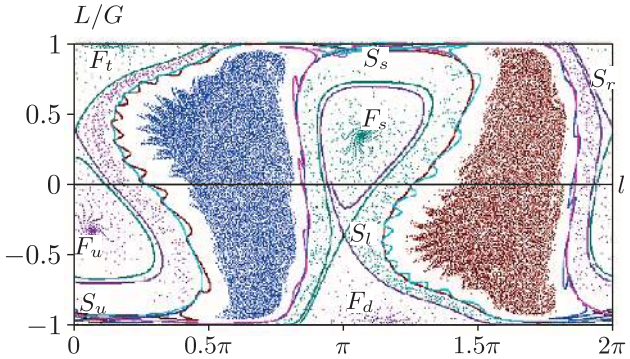

Fig. 5. $a_g = 9.77$. The final position of the invariant manifolds in the Poincaré map.

5.1.1. A Cascade of Local Bifurcations in a Neighborhood of F_n

When $a_g \simeq 9.14$, the focus F_l vanishes due to saddle-node bifurcation, and the stability in the region $\mathfrak{L}$ becomes associated with bifurcations of the focus F_n. In a neighborhood of F_n a transition to chaos is associated with a *cascade of local bifurcations* of the focus F_n. This process is

rather complicated and interesting, therefore we describe it below in detail. By the *cascade of local bifurcations* we mean an infinite sequence of local bifurcations for a fixed or periodic point of focus type. In such cascades *period-doubling bifurcations* can generally alternate with the *Neimark–Sacker bifurcations*.

When $a_g \simeq 8.94$, F_n loses stability due to the Neimark–Sacker bifurcation and becomes an unstable focus. After that the stable invariant curve C_n born from F_n attracts most trajectories in the neighborhood of F_n (see Fig. 6a).

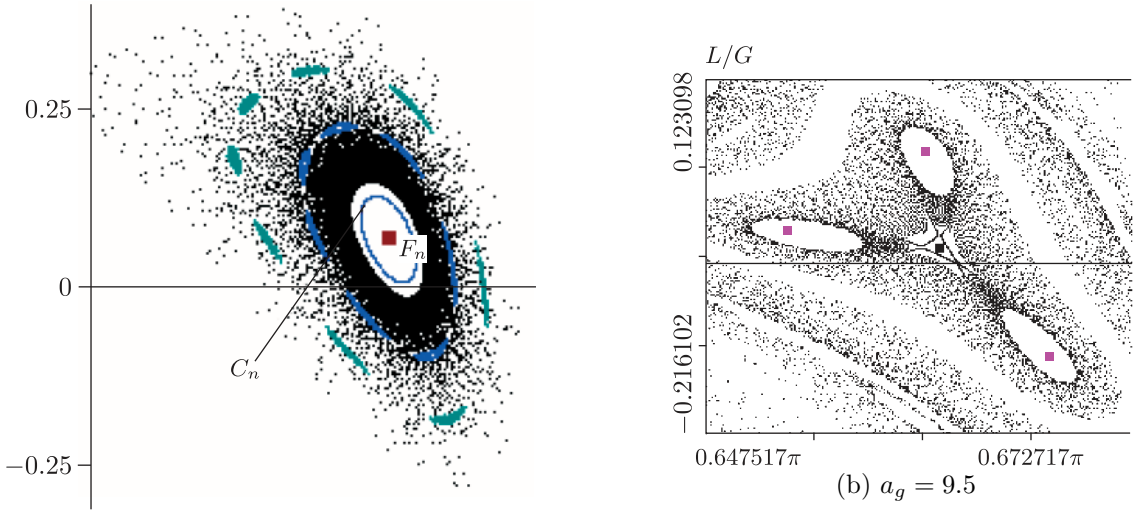

(a) $a_g = 8.94$ (b) $a_g = 9.5$

Fig. 6. The Poincaré maps in a neighborhood of F_n. a) The focus F_n loses stability due to the Neimark–Sacker bifurcation. b) The birth of the unstable 1 : 3 resonance in a neighborhood of F_n.

When $a_g \simeq 9.375$, a resonance of a large period occurs on C_n, and soon C_n disappears according to the *Afraimovich–Shilnikov scenario* [22].

When $a_g = 9.49$, the unstable orbit of period 3 is born in the neighborhood of the unstable F_n (due to occurring of the strong resonance 1 : 3) (see Fig. 6b). After that F_n remains an unstable focus. With further increase in the value of a_g the unstable periodic focus of period 3 becomes a stable periodic focus (due to the Neimark–Sacker bifurcation), and when $a_g \simeq 9.72$, it loses stability due to a cascade of local bifurcations.

The unstable focus F_n bifurcates as well. Since $a_g \simeq 9.634$, two period-doubling bifurcations occur, after which an unstable focus of period 4 is born in the neighborhood of F_n. With further increase in a_g, the last focus of period 4 becomes stable due to the Neimark–Sacker bifurcation. Then the stable focus of period 4 bifurcates due to a cascade of local bifurcations, after which only the focus of period 3 attracts the trajectories in the region $\mathfrak{L}$ (see Fig. 7b).

When $a_g \simeq 9.7715$, the cascade of local bifurcations for the stable focus of period 3 terminates, and our numerical investigation shows that the region $\mathfrak{L}$ does not contain stable fixed or periodic (of not large period) points. This region is entirely filled with chaotic orbits.

Now we describe bifurcations of the focus F_n in more detail. It is well known that the transition to chaos due to a cascade of *period-doubling bifurcations* (also known as the Feigenbaum scenario) is typical of both conservative and dissipative two-dimensional maps continuously depending on a parameter ([23, 24]). The sequence of bifurcational values of parameters converges in this case, and the speed of such convergence (also called the Feigenbaum constant) is asymptotically constant and universal for conservative and dissipative maps.

In our case the beginning of the bifurcations for F_n is the following: 2 period-doubling bifurcations, a Neimark–Sacker bifurcation and a series of 5 period-doubling bifurcations (we could not find bifurcations after the last period-doubling due to numerical miscalculations). We supposed that the subsequence of bifurcations occurring after the Neimark–Sacker bifurcations is subject to

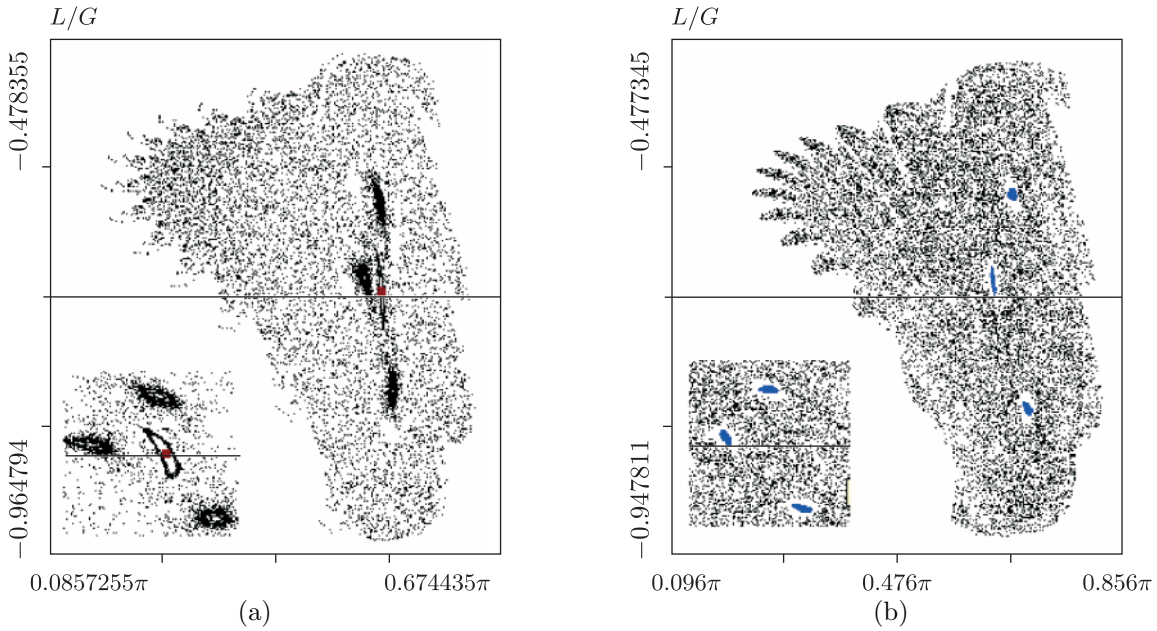

Fig. 7. The Poincaré maps in a neighborhood of F_n (a) before and (b) after the focus F_n bifurcates due to a *cascade of local bifurcations.*

the Feigenbaum scenario and tried to evaluate the speed of convergence by the series of 5 period-doubling bifurcations. However, we could not find a convergence to one of the universal Feigenbaum constants. We assume that this phenomenon is associated with a complex *alternating divergency* of the system (2.2), due to which period-doubling bifurcations compete with the Neimark–Sacker bifurcations. Therefore, in addition to moving in a unit circle through -1, the multipliers of fixed points can also leave this circle through $e^{i\phi}$. Due to this competition the Neimark–Sacker bifurcation can occur after a series of period-doubling bifurcations, which will eventually affect the asymptotical Feigenbaum constant.

5.2. Properties of the Strange Attractor

In this Section we will describe qualitative and quantitative characteristics of the chaotic set in the region $\mathfrak{L}$.

The attractive region of the strange attractor is formed by uniting $\mathfrak{L}$ and $\mathfrak{R}$. The location of the stable invariant manifolds of saddle points helps to construct the boundary of the strange attractor. On the left the attractor is bounded by the stable invariant manifold (light blue) of the saddle S_r, and on the right the attractor is bounded by the stable invariant manifold (dark blue) of S_l (see Fig. 5). In the upper and lower parts of the Poincaré map these manifolds approach each other as if to close the region of the strange attractor. Thus, almost all trajectories starting from $\mathfrak{R}$ evolve into $\mathfrak{L}$ and wander about in the strange attractor.

In what follows we analyze the *Lyapunov exponents* of the strange attractors for the flow system (2.2). For our system, 3 of 6 Lyapunov exponents are zero due to the existence of 3 first integrals (2.4). The fourth Lyapunov exponent is responsible for a shift in time and hence is zero, too. Thus, the trajectories of the system generally admit two non-zero Lyapunov exponents. We use the well-known *Binettin algorithm* [25] to calculate a full spectrum of the Lyapunov exponents.

To evaluate the numerical miscalculations, we compute the spectrum of the Lyaponov exponents many times from different points of the attractor. Then we consider the calculated set as a sampling of a random variable, for which we evaluate the expectation value and sample variance of the Lyapunov exponents. The non-zero Lyapunov exponents with evaluation of the numerical miscalculations and their sum are shown below:

$$\begin{aligned} \Lambda_1 &= 0.083368 \pm 0.000422, \\ \Lambda_2 &= -0.084553 \pm 0.000423, \\ \Lambda_1 + \Lambda_2 &= -0.001184 \pm 0.000011. \end{aligned} \tag{5.2}$$

The positive Lyapunov exponent proves the chaotic nature of the attractor, while the negative sum of the Lyapunov exponents points to the compression of volume, which is characteristic of the typical attractors. Note that this compression in our strange attractor is very weak due to small values of the sum of the Lyapunov exponents.

Now we calculate the *Kaplan–Yorke dimension* [16] of the strange attractor:

$$D = 1 + \frac{\Lambda_1}{|\Lambda_2|} \simeq 1.986. \tag{5.3}$$

This formula shows that the Kaplan–Yorke dimension is close to 2, which explains why the area of the attractor is comparable with the area of the phase space of (3.3).

The described properties imply that the discovered stable chaotic set in the region $\mathfrak{L}$ is a genuine strange attractor. However, this attractor is not related to one of the well-known attractors, such as the attractors of Lorenz or Henon type. Due to the weak dissipation the attractor may be classified as a *weak strange attractor*. The attractor of this type is presented in [26].

6. MIXED DYNAMICS

As was mentioned above, when the center of mass of the ball is displaced along two axes, the system (2.2) admits an additional involution corresponding to the reflection of the ball with respect to the plane passing through the axes of displacement. For the Poincaré map this involution is reduced to one of three involutions of the set (4.8). In this case we have found another interesting type of chaotic behavior — the so-called *mixed dynamics* [27, 28] (see also [18] where this phenomenon is pointed out for the nonholonomic model of Celtic stone). Here we give this definition only for two-dimensional reversible maps. In this case, *mixed dynamics* is a closed chaotic set of orbits with the following properties:

- This set contains a countable set of asymptotically stable, asymptotically unstable, saddle and symmetric elliptic orbits.
- The closure of the sets of orbits of different types has a non-empty intersection.

The latter property means that attractors and repellers can intersect each other. Moreover, in the numerical experiments an attractor and a repeller can form a single whole.

Following [29], by an *attractor* we will mean a set of *images of a fixed line* of the involution iterated in forward time and, accordingly, by a *repeller* we will mean a set of such images iterated in backward time.

The experimental evidence of the fact that a closed chaotic set has a mixed nature is that an *attractor* and a *repeller* differ due to the asymmetry of the asymptotically stable orbits belonging to the *attractor* and the asymptotically unstable orbits belonging to the *repeller*.

Since we iterate a *fixed line* of an involution, symmetric periodic (elliptic and saddle) orbits also belong to this intersection [11]. Moreover, asymptotically stable and unstable periodic orbits should generically present in any neighborhood of this intersection. However, it is impossible to find all these orbits in numerical investigations. Hence, instead orbits of large period we tried to find periodic orbits of any period. In addition, we have replaced the requirement of an intersection of the closures of stable and unstable orbits with the requirement of vicinity of these orbits.

Figures 8a and 8b show, respectively, the attractor and the repeller obtained by iterating the *fixed line* forward and backward [1)] for the following values of parameters:

$$\begin{gathered} E = 50, a_g = 9.7715, \\ R = 3, m = 1, \\ I_1 = 1, I_2 = 2, I_3 = 3, \\ a_1 = 1, a_2 = 1.5, a_3 = 0, g = \pi/2. \end{gathered} \tag{6.1}$$

For convenience, we divide each of the figures (8a and 8b) into two parts. Two large "white" regions belong to the first part. These "white" regions are associated with dissipative dynamics.

[1)] Figures 8a and 8b show, respectively, 100 forward and backward iterations for points of the line $L/G = 0$ with the step 0.001.

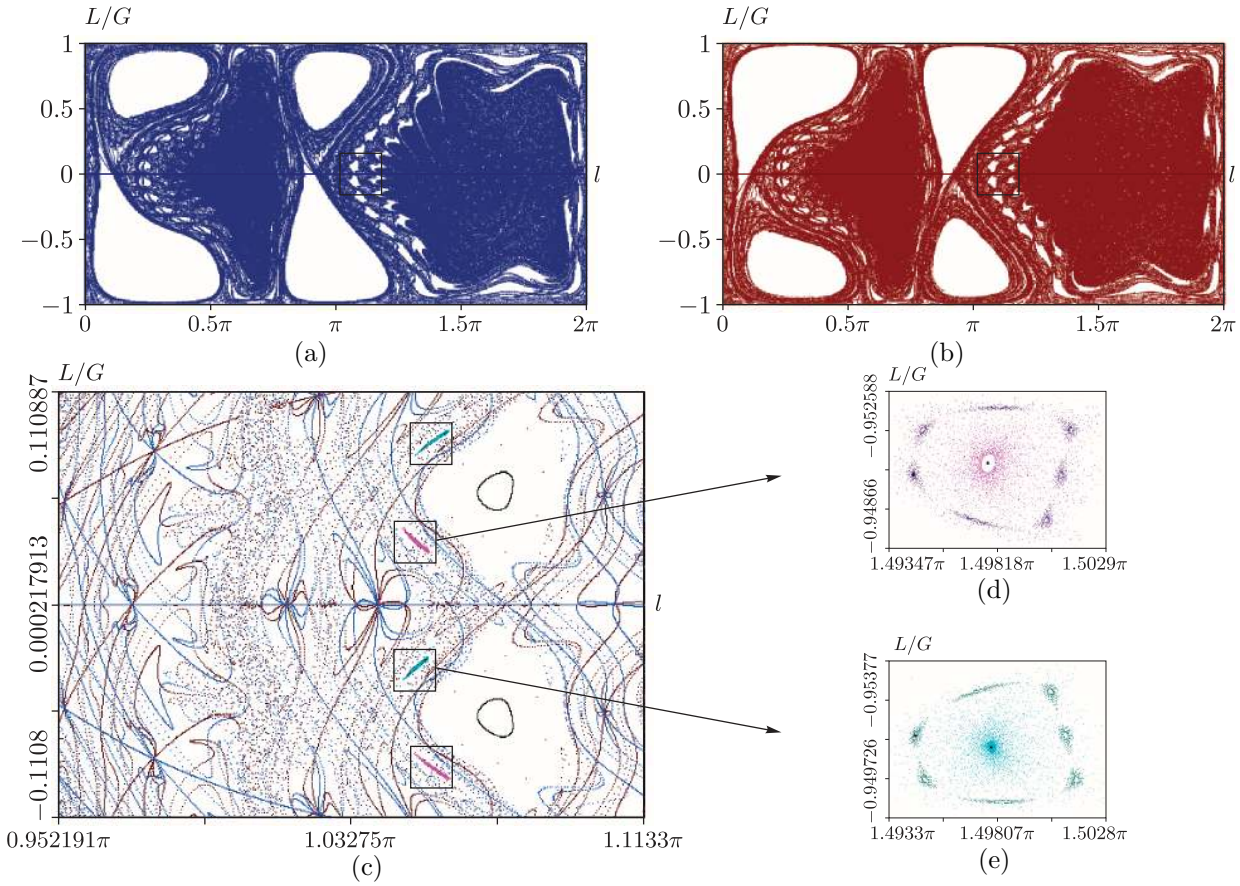

Fig. 8. The Poincaré maps. a) An *attractor* with 100 forward iterations of the Poincaré map for points of the line $L/G = 0$ with the step 0.001. b) A *repeller* with 100 backward iterations of the Poincaré map for points of the line $L/G = 0$ with the step 0.001. c) A zoomed region (indicated with a rectangle from Figs. (a) and (b)) containing orbits of both the *attractor* and the *repeller*. d) A zoomed region of the unstable points of period 19 (in the center of the figure) and 133 (surrounding the foci of period 19). e) A zoomed region of the stable points of period 19 (in the center of the figure) and 133 (surrounding the foci of period 19).

Trajectories starting from the lower part of these regions (from the neighborhood of unstable foci) pass to the stable foci of the upper part of these regions. Moreover, these two regions are invariant in the sense that the orbits cannot leave them and cannot evolve into them from outside.

The second part contains a region with chaotic dynamics.It can be seen that the chaos in the second part of Fig. 8a differs from the chaos in the second part of Fig. 8b. However, these two parts have a non-empty intersection. In addition, we find stable and unstable periodic points of period 19 and 133 inside this chaos. Moreover, the stable periodic points are close to the unstable ones (see Figs. 8c-e). Figure 8c shows a zoomed region (indicated with a rectangle in Figs. 8a and 8b) containing orbits of both the *attractor* and the *repeller*. Figures 8d and 8e show a zoomed region, respectively, of the unstable and stable points of period 19 (in the center of the figures) and 133 (surrounding the foci of period 19).

Remark 4. Small "white" regions in Figs. 8a–b and large "white" regions in Fig. 8c contain periodic elliptic orbits. Why do the *images of fixed lines* not evolve into these regions? We suppose that the answer is quite simple. We iterate only the *fixed line* of the involution σ_1 from the set (4.8). But it is well known [11] that if a map (or a system) is reversible with respect to the involution σ, then this map is also reversible with respect to the involution $\mathcal{F}_{g_0}^{-1}\sigma$. But it is difficult to find and iterate the *fixed line* of this involution, so we have not dealt with it. Thus, we assume that the above-mentioned "white" regions will be filled with such iterations of the *fixed line* of the involution $\mathcal{F}_{g_0}^{-1}\sigma$.

All these facts confirm that the chaotic dynamics under consideration is *mixed dynamics*.

ACKNOWLEDGMENTS

The author thanks A. V. Borisov, S. V. Gonchenko, S. P. Kuznetsov, I. S. Mamaev and I. R. Sataev for fruitful discussions and comments.

This work was supported by the RFBR grants No. 13-01-00589 and 13-01-97028-povolzhye, the Federal Target Program "Personnel" No.14.B37.21.0361, and by the Federal Target Program "Scientific and Scientific-Pedagogical Personnel of Innovative Russia" (Contract No. 14.B37.21.0863).

REFERENCES

1. Ehlers, K. and Koiller, J., Rubber Rolling: Geometry and Dynamics of $2-3-5$ Distributions, in *Proc. IUTAM Symposium 2006 on Hamiltonian Dynamics, Vortex Structures, Turbulence (Moscow, Russia, 25–30 August 2006),* pp. 469–480.
2. Koiller, J. and Ehlers, K. M., Rubber Rolling over a Sphere, *Regul. Chaotic Dyn.,* 2007, vol. 12, no. 2, pp. 127–152.
3. Hadamard, J., Sur les mouvements de roulement, *Mémoires de la Société des sciences physiques et naturelles de Bordeaux, 4 sér.,* 1895, vol. 5, pp. 397–417.
4. Borisov, A. V., Mamaev, I. S., and Bizyaev, I. A., The Hierarchy of Dynamics of a Rigid Body Rolling without Slipping and Spinning on a Plane and a Sphere, *Regul. Chaotic Dyn.,* 2013, vol. 18, pp. 227–328.
5. Bizyaev, I. A. and Kazakov, A. O., Integrability and Stochastic Behavior in Some Nonholonomic Dynamics Problems, *Rus. J. Nonlin. Dyn.,* 2013, vol. 9, no. 2, pp. 257–265 (Russian).
6. Borisov, A. V. and Mamaev, I. S., Conservation Laws, Hierarchy of Dynamics and Explicit Integration of Nonholonomic Systems, *Regul. Chaotic Dyn.,* 2008, vol. 13, no. 5, pp. 443–490.
7. Bolsinov, A. V., Borisov, A. V., and Mamaev, I. S., Rolling of a Ball without Spinning on a Plane: The Absence of an Invariant Measure in a System with a Complete Set of Integrals, *Rus. J. Nonlin. Dyn.,* 2012, vol. 8, no. 3, pp. 605–616 [*Regul. Chaotic Dyn.,* 2012, vol. 17, no. 6, pp. 571–579].
8. Borisov, A. V. and Mamaev, I. S., *Rigid Body Dynamics: Hamiltonian Methods, Integrability, Chaos,* Moscow–Izhevsk: R&C Dynamics, Institute of Computer Science, 2005 (Russian).
9. Borisov, A. V. and Mamaev, I. S., Rolling of a Rigid Body on a Plane and Sphere: Hierarchy of Dynamics, *Regul. Chaotic Dyn.,* 2002, vol. 7, no. 2, pp. 177–200.
10. Borisov, A. V., Mamaev, I. S., and Kilin, A. A., The Rolling Motion of a Ball on a Surface: New Integrals and Hierarchy of Dynamics, *Regul. Chaotic Dyn.,* 2002, vol. 7, no. 2, pp. 201–219.
11. Chavoya-Aceves, O. and Piña, E., Symmetry Lines of the Dynamics of a Heavy Rigid Body with a Fixed Point, *Il Nuovo Cimento B,* 1989, vol. 103, no. 4, pp. 369–387.
12. Devaney, R. L., Reversible Diffeomorphisms and Flows, *Trans. Amer. Math. Soc.,* 1976, vol. 218, pp. 89–113.
13. Gonchenko, S. V., Lamb, J. S. W., Rios, S., Turaev, D., Attractors and Repellers near Generic Reversible Elliptic Points, *arXiv:1212.1931v1 [math. DS],* 9 Dec. 2012, pp. 1–11.
14. Borisov, A. V. and Mamaev, I. S., Strange Attractors in Rattleback Dynamics, *Uspekhi Fiz. Nauk,* 2003, vol. 173, no. 4, pp. 408–418 [*Physics–Uspekhi,* 2003, vol. 46, no. 4, pp. 393–403].
15. Borisov, A. V., Kilin, A. A. and Mamaev, I. S., New Effects in Dynamics of Rattlebacks, *Doklady Physics.–MAIK Nauka/Interperiodica,* 2006, vol. 51, no. 5, pp. 272–275.
16. Borisov, A. V., Jalnine, A. Yu., Kuznetsov, S. P., Sataev, I. R., and Sedova, J. V., Dynamical Phenomena Occurring Due To Phase Volume Compression in Nonholonomic Model of the Rattleback, *Regul. Chaotic Dyn.,* 2012, vol. 17, no. 6, pp. 512–532.
17. Gonchenko, A. S., Gonchenko, S. V., and Kazakov, A. O., On Some New Aspects of Celtic Stone Chaotic Dynamics, *Rus. J. Nonlin. Dyn.,* 2012, vol. 8, no. 3, pp. 507–518 (Russian).
18. Gonchenko, A. S., Gonchenko, S. V., and Kazakov, A. O., Richness of Chaotic Dynamics in the Nonholonomic Model of Celtic Stone, *Regul. Chaotic Dyn.,* 2013, vol. 18, no. 5, pp. 521–538.
19. Kazakov, A. O., Chaotic Dynamics Phenomena in the Rubber Rock-n-Roller on a Plane Problem, *Rus. J. Nonlin. Dyn.,* 2013, vol. 9, no. 2, pp. 309–325 (Russian).
20. Gonchenko, S. V., Simó, C., and Vieiro, A., Richness of Dynamics and Global Bifurcations in Systems with a Homoclinic Figure-Eight, *Nonlinearity,* 2013, vol. 26, no. 3, pp. 621–678.
21. Lukyanov, V. I. and Shilnikov, L. P., On Some Bifurcations of Dynamical Systems with Homoclinic Structures, *Dokl. Akad. Nauk SSSR,* 1978, vol. 243, no. 1, pp. 26–29 [*Soviet Math. Dokl.,* 1978, vol. 19, pp. 1314–1318].
22. Afraimovich, V. S. and Shilnikov, L. P., On Some Global Bifurcations Connected with the Disappearance of a Fixed Point of Saddle-Node Type, *Dokl. Akad. Nauk SSSR,* 1974, vol. 219, no. 6, pp. 1281–1285 [*Soviet Math. Dokl.,* 1974, vol. 15, no. 3, pp. 1761–1765].
23. Feigenbaum, M. J., Universal Behavior in Nonlinear Systems: Order in Chaos (Los Alamos, N. M., 1982), *Phys. D,* 1983, vol. 7, nos. 1–3, pp. 16–39.

24. Borisov, A. V. and Simakov, N. N., Period Doubling Bifurcation in Rigid Body Dynamics, *Regul. Chaotic Dyn.,* 1997, vol. 2, no. 1, pp. 64–74 (Russian).
25. Benettin, G., Galgani, L., Giorgilli, A., and Strelcyn, J.-M., Lyapunov Characteristic Exponents for Smooth Dynamical Systems and for Hamiltonian Systems: A Method for Computing All of Them: P. 1: Theory; P. 2: Numerical Application, *Meccanica,* 1980, vol. 15, pp. 9–30.
26. Felk, E. V. and Savin, A. V. The Effect of Weak Nonlinear Dissipation on the Stochastic Web, in Proc. of the Conf. "Dynamics, Bifurcations and Strange attractors" (Nizhny Novgorod, Russia, 2013), pp. 36–37.
27. Lamb, J. S. W. and Stenkin, O. V., Newhouse Regions for Reversible Systems with Infinitely Many Stable, Unstable and Elliptic Periodic Orbits, *Nonlinearity,* 2004, vol. 17, no. 4, pp. 1217–1244.
28. Delshams, A., Gonchenko, S. V., Gonchenko, A. S., Lázaro, J. T., and Sten'kin, O., Abundance of Attracting, Repelling and Elliptic Periodic Orbits in Two-Dimensional Reversible Maps, *Nonlinearity,* 2013, vol. 26, no. 1, pp. 1–33.
29. Pikovsky, A. and Topaj, D., Reversibility vs. Synchronization in Oscillator Latties, *Phys. D,* 2002, vol. 170, pp. 118–130.